

Behavior Foundation Model for Humanoid Robots

Weishuai Zeng^{1,5}, Shunlin Lu^{2,5}, Kangning Yin^{3,5}, Xiaojie Niu⁵, Minyue Dai^{4,5}, Jingbo Wang⁵, Jiangmiao Pang⁵

¹Peking University, ²The Chinese University of Hong Kong, Shenzhen

³Shanghai Jiaotong University, ⁴Fudan University, ⁵Shanghai Artificial Intelligence Laboratory

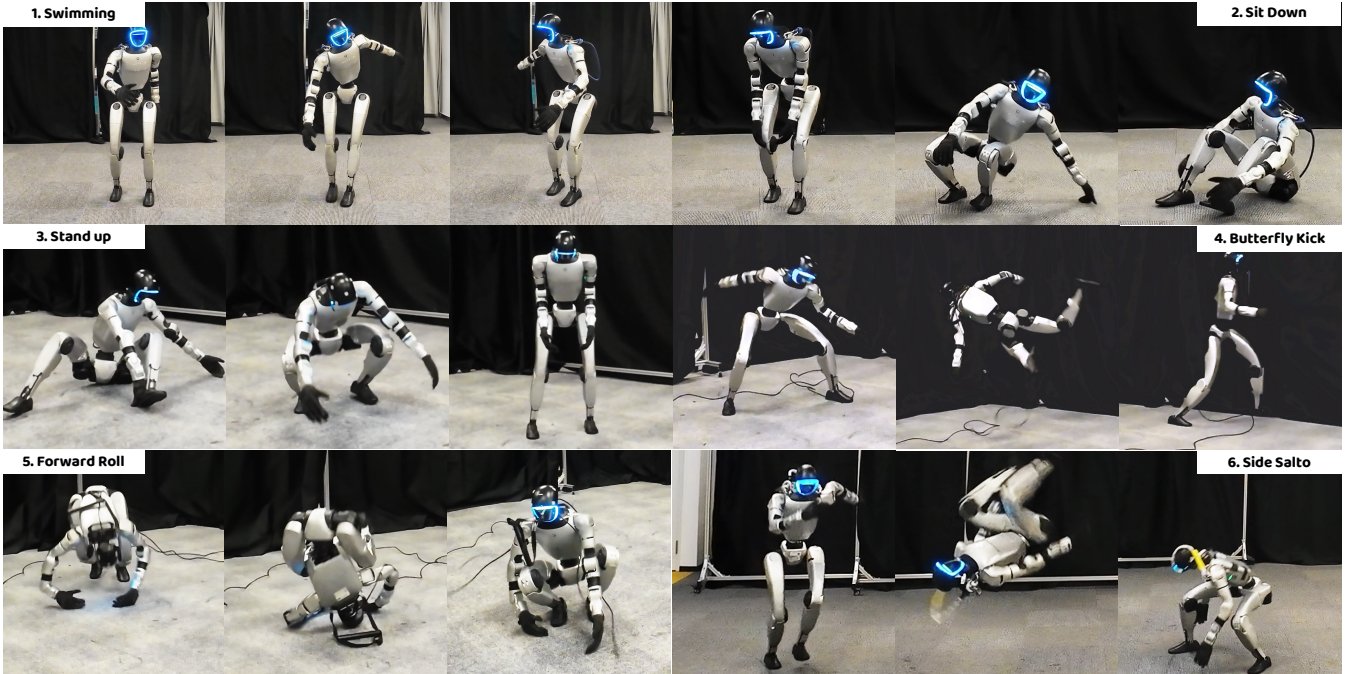


Fig. 1: **Behavior Foundation Model** enables humanoid robots to perform a variety of behaviors in a zero-shot manner, including (1) a swimming pose, (2) sitting down on the ground, (3) standing up from the ground, and (4) butterfly kick. It also facilitates efficient acquisition of new behaviors such as (5) a forward roll and (6) a side salto.

Abstract—Whole-body control (WBC) of humanoid robots has witnessed remarkable progress in skill versatility, enabling a wide range of applications such as locomotion, teleoperation, and motion tracking. Despite these achievements, existing WBC frameworks remain largely task-specific, relying heavily on labor-intensive reward engineering and demonstrating limited generalization across tasks and skills. These limitations hinder their response to arbitrary control modes and restrict their deployment in complex, real-world scenarios. To address these challenges, we revisit existing WBC systems and identify a shared objective across diverse tasks: the generation of appropriate behaviors that guide the robot toward desired goal states. Building on this insight, we propose the Behavior Foundation Model (BFM), a generative model pretrained on large-scale behavioral datasets to capture broad, reusable behavioral knowledge for humanoid robots. BFM integrates a masked online distillation framework with a Conditional Variational Autoencoder (CVAE) to model behavioral distributions, thereby enabling flexible operation across arbitrary control modes and efficient acquisition of novel behaviors without retraining from scratch. Extensive experiments in both simulation and on a physical humanoid platform demonstrate that BFM generalizes robustly across diverse WBC tasks while rapidly adapting to new behaviors. These results establish BFM as a promising step toward a foundation model for general-purpose humanoid control. Videos and supplementary materials are available at: bfm4humanoid.github.io ..

I. INTRODUCTION

Humanoid robots are capable of executing a wide range of whole-body control (WBC) tasks, including language interaction [1, 2], human teleoperation [3–5] and whole-body motion tracking [6, 7]. Despite this versatility, most existing WBC systems are typically designed for specific control modes. For example, a motion tracking policy accepts only reference motions, whereas a locomotion policy responds exclusively to velocity commands. Such rigid specialization of control modes hinders cross-task generalization: a locomotion policy, for instance, cannot directly exploit reference motions for whole-body tracking. Recent studies have attempted to support multiple control modes with mask strategies. However, these approaches are either confined to simplified virtual avatars [8] or prioritize a fixed set of control modes [9], thus failing to accommodate arbitrary control modes on real humanoid robots. We argue that the root cause of this limitation lies in the absence of a unified formulation across diverse tasks. To address this challenge, we revisit the design of existing WBC systems and make a key observation: although control modes differ, the resulting outcomes of these systems, whether walking or dancing, are all fundamentally **behaviors** of humanoid robots, which naturally serve as a unified formulation across diverse tasks.

Under this perspective, task-specific control modes, whether velocity commands, VR signals or reference motions can all be interpreted as distinct specifications of the behaviors.

One behavior can often be specified through multiple control modes. A simple yet illustrative example is that the behavior of walking forward can be learned under both locomotion and motion tracking settings. This observation suggests that, despite variations in control modes, existing WBC systems ultimately pursue a shared objective: the generation of appropriate behaviors. Such a perspective motivates the decoupling of behaviors from control modes, thereby shifting the paradigm from isolated task learning toward holistic behavior learning. Inspired by the success of foundation models in other domains [10], if we may pretrain a foundation model on large and diverse behavioral datasets, it may encode a broad spectrum of behavioral knowledge, which can then be applied to a variety of downstream tasks.

To this end, we introduce the **Behavior Foundation Model (BFM)** for humanoid robots, a generative model pretrained on large-scale behavioral datasets to capture broad and reusable behavioral knowledge. BFM can be directly steered by diverse control modes to accomplish corresponding tasks, while also enabling the efficient acquisition of novel behaviors without the need of retraining from scratch. In general, BFM establishes a flexible and generalizable framework for humanoid control, highlighting its potential as a foundation for the next generation of WBC system design.

To realize this vision, we first adopt motion imitation as a common abstraction of behaviors to train a proxy agent in simulation. Then, we pretrain BFM using a masked online distillation framework combined with a Conditional Variational Autoencoder (CVAE) [11], which provides a versatile control interface capable of supporting diverse control modes as well as a structured latent space that facilitates both behavior composition and modulation. Furthermore, we integrate residual learning [12] into our framework, enabling efficient acquisition of novel behaviors by leveraging the behavioral knowledge already encoded in the BFM. As presented in Figure 1, the overall framework demonstrates both versatility and robustness in real-world deployment.

In summary, our contributions are threefold: 1) we present Behavior Foundation Model for humanoid robots, shifting the focus of humanoid control from holistic task learning to unified behavior learning; 2) we demonstrate our framework integrating masked online distillation and CVAE can be directly steered for diverse WBC tasks and may efficiently acquire new behaviors via residual learning without retraining from scratch; 3) extensive experiments in both simulation and on a real humanoid robot validate expressiveness and effectiveness of our BFM, highlighting its potential as a foundation for developing general-purpose humanoid robots.

II. RELATED WORK

A. Humanoid Whole-body Control

Existing WBC systems for humanoids can be generally categorized by their control modes ranging from abstract to concrete. The most abstract control mode is natural

language [1, 2] which may correspond to a series of feasible behaviors that all satisfy the given instructions. A more concrete and widely adopted control mode, especially for locomotion and loco-manipulation, involves the velocity commands and base height commonly combined with other signals like gait and posture [13], upper-body joint positions from exo-skeleton [4] or VR devices with inverse kinematics (IK) [5]. Besides processing VR signals with IK, other teleoperation systems [3] directly map kinematic data from VR controllers to the humanoid, enabling highly expressive and accurate whole-body control. The most concrete control mode for existing WBC systems is motion tracking which provides nearly complete information about the reference pose either from offline datasets [7] or online motion capture systems [14]. While these systems produce impressive results, their control mode is often determined at design time and therefore lack cross-task generalization. HOVER [9] attempts to address this by employing a unified policy with a masking strategy to achieve multi-modal control, demonstrating versatile humanoid control across diverse WBC tasks.

B. Behavior Foundation Model

Recent advances in reinforcement learning has led to Behavior Foundation Models, which exhibit versatile behavior generation and strong generalization across diverse tasks. Existing works have implemented BFM from distinct perspectives. Motivo [15] and its series of works use forward-backward representations to enable unsupervised learning on reward-free transitions, yielding near-optimal policies for zero-shot inference across diverse tasks. MaskedMimic [8] and HOVER [9] employ online masked distillation to train goal-conditioned policies, which also allows zero-shot generalization across tasks and contexts. Our framework draws inspiration from the latter line of work but differs in key aspects. HOVER’s two-stage mask strategy still prioritizes specific control modes, while our BFM supports arbitrary modes through direct application of sparsity mask. Masked-mimic focuses on simplified virtual avatars and lacks the latent space analysis to clarify advantages of CVAE over other generative models, while our BFM targets real-world humanoids and reveals the latent space properties for applications like behavior composition and modulation. Through both theoretical and empirical contributions, our BFM offers a systematical analysis of the underlying unified formulation existing models have actually learned and enables a wide range of downstream applications on real humanoid robots.

III. PROXY AGENT TRAINING

A. Behaviors under Reinforcement Learning Formulation

We formulate the problem of humanoid control as a goal-conditioned reinforcement learning (RL) task, where a policy π is trained to achieve certain objectives. The state s_t comprises both the humanoid’s proprioception s_t^p and the goal state s_t^g . Using the humanoid’s proprioception s_t^p and the goal state s_t^g , the reward function is defined as $r_t = R(s_t^p, s_t^g)$ for policy optimization. The action a_t represents the target joint positions for humanoids, which are then fed into the PD

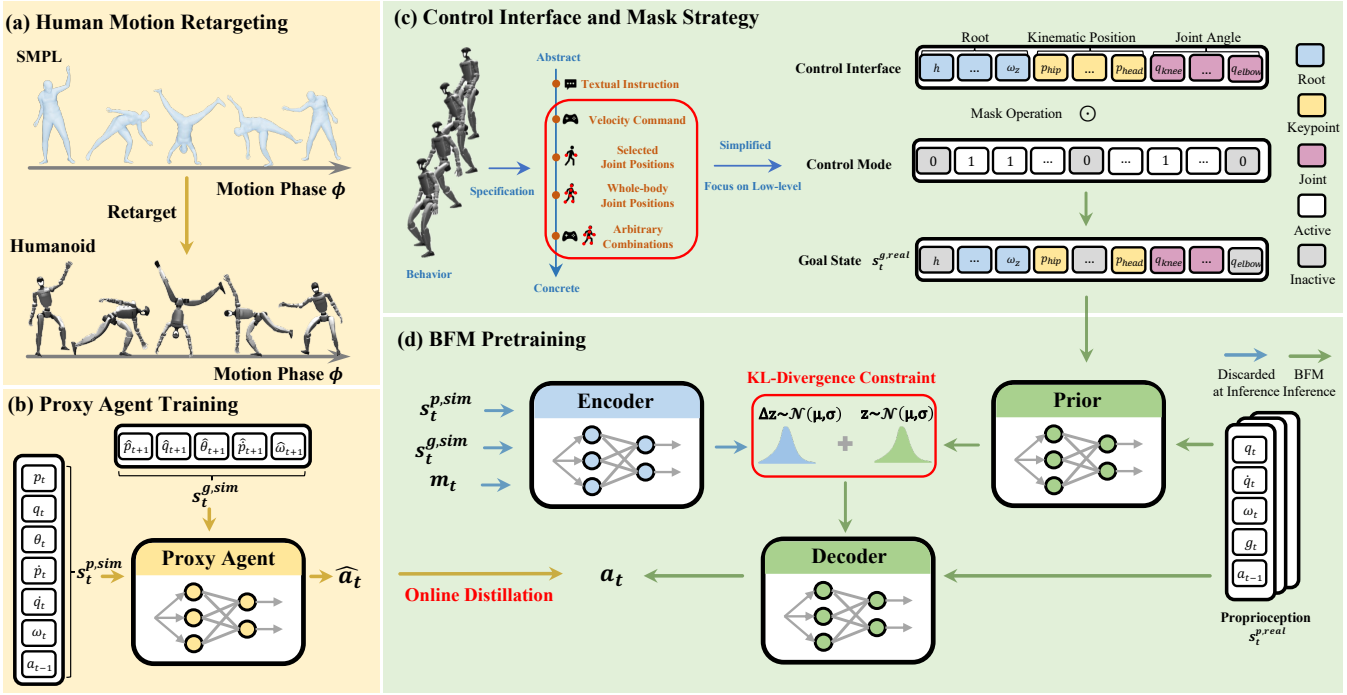


Fig. 2: Overview of BFM Implementation. (a) Human motion dataset is retargeted to humanoid robots for proxy agent training. (b) The proxy agent is trained via motion imitation which has access to all information in simulators. (c) One behavior can be specified in multiple control modes from abstract textual instructions to concrete whole-body joint positions, resulting distinct goal states. We simplify the activation of distinct control modes to applying mask to a unified control interface. This interface is restricted to the union of root, kinematic position, and joint angle, emphasizing our focus on low-level humanoid control. (d) We model the BFM with a CVAE and employ the DAgger framework for BFM pretraining, providing a structured latent space to encode extensive behavioral knowledge.

controller to actuate the robot’s degrees of freedom. Proximal Policy Optimization (PPO) algorithm [16] is employed to maximize the cumulative reward $E[\sum_{t=1}^T \gamma^{t-1} r_t]$.

With the formulation above, we define behaviors as *trajectories over the humanoid’s proprioceptive states and actions*. We particularly exclude task-related goal states s_t^g from trajectories, as we interpret them as external motives that drive the generation of appropriate behaviors. Such exclusion avoids pre-determination of control modes, allowing behaviors to be a unified formulation for humanoid control.

In order to distinguish the observable states during real-world deployment from the privileged states in simulators, we use $s_t^{p,sim}$ and $s_t^{g,sim}$ to represent privileged states in simulators and $s_t^{p,real}$ and $s_t^{g,real}$ to represent observable states available during real-world deployment. With such notations, the behavior is defined as trajectories over $s_t^{p,real}$ and a_t , expressed as $\tau = [s_1^{p,real}, a_1, s_2^{p,real}, \dots, s_{T-1}^{p,real}, a_{T-1}, s_T^{p,real}]$.

B. Human Motion Retargeting

Human motion dataset plays an important role in humanoid behavioral dataset preparation for their diversity and high quality. We select the publicly available AMASS dataset [17] where each motion sample is parameterized by the SMPL model [18]. To bridge the embodiment gap between SMPL human model and humanoid robots, we employ a two-stage retargeting approach [19]. First, we optimize the shape parameter of SMPL model for humanoid robots by minimizing distances between selected links in

the rest pose. Second, we optimize the humanoid’s root translation, orientation and joint positions by minimizing distances between selected links throughout the whole sequence. Additional regularization terms are added to avoid aggressive behaviors and ensure temporal smoothness.

Unlike previous works which use a motion imitator trained with privileged information in simulators to further filter the dataset, we directly use the raw dataset for BFM pretraining.

C. Proxy Agent Training via Motion Imitation

Instead of organizing behavioral dataset as offline trajectories for BFM pretraining, we train a proxy agent denoted as π^{proxy} using motion imitation. The obtained proxy agent may provide actions given the current proprioceptive state and goal state derived from the reference motion, which may generate quantities of behavioral data by online rolling out.

State Space Design. The state space of the proxy agent is comprised of the privileged proprioception and goal state in simulators. The privileged proprioception for proxy agent is defined as $s_t^{p,sim} \triangleq [p_t, q_t, \theta_t, \dot{p}_t, \dot{q}_t, \omega_t, a_{t-1}]$, which contains the humanoid rigid-body position p_t , joint position q_t , orientation θ_t , linear velocity \dot{p}_t , joint velocity \dot{q}_t , angular velocity ω_t and previous action a_{t-1} . The privileged goal state is defined as $s_t^{g,sim} \triangleq [\hat{p}_{t+1} - p_t, \hat{q}_{t+1} - q_t, \hat{\theta}_{t+1} \ominus \theta_t, \hat{v}_{t+1} - v_t, \hat{\omega}_{t+1} - \omega_t, \hat{p}_{t+1} - p_t^{root}, \hat{\theta}_{t+1} \ominus \theta_t^{root}]$, which contains the one-frame difference between the reference pose ($\hat{p}_{t+1}, \hat{q}_{t+1}, \hat{\theta}_{t+1}, \hat{v}_{t+1}, \hat{\omega}_{t+1}$) and the current pose. p_t^{root}

TABLE I: Reward Designs for Proxy Agent

Term	Weight	Term	Weight
Task Reward			
Body position	1.0	Body position (selected keypoint)	1.6
Body position (feet)	2.1	Body rotation	0.5
Body velocity	0.5	Body angular velocity	0.5
DoF position	0.75	DoF velocity	0.5
Penalty			
Torque limits	-5.0	DoF position	-10.0
Dof Velocity	-5.0	Termination	-200.0
Regularization			
Torque	-0.000001	Action rate	-0.5
Feet orientation	-2.0	Feet heading alignment	-0.02
Feet air time	-10.0	Slippage	-1.0
Hip pos	-1.0	Close feet distance	-0.5

TABLE II: Domain Randomization

Term	Value	Term	Value
Dynamics			
Base CoM offset	$\mathcal{U}(-0.1, 0.1)$	Link mass	$\mathcal{U}(0.9, 1.1) \times \text{default}$
Friction	$\mathcal{U}(0.5, 1.2)$	P gain	$\mathcal{U}(0.9, 1.1) \times \text{default}$
D gain	$\mathcal{U}(0.9, 1.1) \times \text{default}$	Torque RFI [20]	0.05 × torque limit
External Perturbations			
Push interval	[5, 10]	Max push velocity	1.0

refers to the root translation and θ_t^{root} refers to the root orientation of the current pose. All these goal states are rotated to the local coordinate of the current frame.

Reward Design and Domain Randomization. We formulate the reward r_t as a weighted sum of three components: 1) task rewards for motion imitation, 2) regularization, and 3) penalty, as detailed in Table I. We employ curriculum learning to the regularization and penalty terms, encouraging the policy to focus on motion imitation initially and gradually leverage penalty and regularization to shape the behaviors. We also apply domain randomization during training by randomizing dynamics and applying external perturbations. Details of domain randomization are listed in table II.

Reference State Initialization and Early Termination. Proper initialization is crucial for motion imitation. We employ the Reference State Initialization (RSI) framework [21], where the starting point of the reference motion is randomly sampled and the robot’s initial state is derived from the corresponding reference pose. To facilitate efficient training, we implement early termination to avoid collecting invalid data. Unlike previous works that rely on multiple termination conditions (e.g., gravity, height), we simplify the conditions to a single tracking tolerance: the episode terminates if the average link distance between the robot and reference pose exceeds certain threshold. This design avoids direct termination when the gravity or height termination conditions are triggered after RSI (e.g. getting up from the ground).

Hard Negative Mining and Motion Filtering. When training on large datasets, the motion imitation policy may converge to an average point, thereby hindering full coverage of the whole dataset. To address this issue, we employ the strategy of hard negative mining by periodically evaluating our policy over the entire dataset and dynamically adjusting the sampling probability for each motion sample. If the policy fails to track a particular sample, its sampling probability is increased by a predefined factor, whereas

successful tracking leads to a corresponding decrease. When the policy’s success rate over the entire dataset plateaus and ceases to improve, we apply a filtering mechanism to the original motion dataset. This process identifies samples that persistently fail to be learned, classifying them as implausible instances beyond the capabilities of the current proxy agent.

IV. BFM PRETRAINING

A. BFM under Reinforcement Learning Formulation

The Behavior Foundation Model is a generative model tasked with learning the underlying distribution of demonstrated behaviors, $\bar{P}(\tau)$. Under the Markov assumption, the pretraining objective reduces to maximizing the expected log-likelihood over the dataset $\mathcal{D} = \{(s_i^{p,real}, a_i)\}_{i=1}^M$ of M state-action pairs by optimizing the model parameters θ :

$$\max_{\theta} E_{(s_t^{p,real}, a_t) \sim \mathcal{D}} [\log \pi_{\theta}(a_t | s_t^{p,real})] \quad (1)$$

A monolithic policy $\pi_{\theta}(a_t | s_t^{p,real})$ is ineffective for control. We introduce the goal state $s_t^{g,real}$ and express the policy as a marginalization over possible goal states in the dataset:

$$\begin{aligned} \log \pi_{\theta}(a_t | s_t^{p,real}) &= \log E_{s_t^{g,real} \sim p(s_t^{g,real} | s_t^{p,real})} [\pi_{\theta}(a_t | s_t^{p,real}, s_t^{g,real})] \\ &\quad [\pi_{\theta}(a_t | s_t^{p,real}, s_t^{g,real})] \end{aligned} \quad (2)$$

By applying the Jensen Inequality, we may obtain a tractable lower bound as a surrogate of the original objective:

$$\begin{aligned} \log E_{s_t^{g,real} \sim p(s_t^{g,real} | s_t^{p,real})} [\pi_{\theta}(a_t | s_t^{p,real}, s_t^{g,real})] \\ \geq E_{s_t^{g,real} \sim p(s_t^{g,real} | s_t^{p,real})} [\log \pi_{\theta}(a_t | s_t^{p,real}, s_t^{g,real})] \end{aligned} \quad (3)$$

The complete pretraining objective for our BFM is then to maximize the lower bound over the entire dataset:

$$\max_{\theta} E_{(s_t^{p,real}, a) \sim \mathcal{D}} [E_{s_t^{g,real} \sim p(s_t^{g,real} | s_t^{p,real})} [\log \pi_{\theta}(a_t | s_t^{p,real}, s_t^{g,real})]] \quad (4)$$

B. Real-world Proprioception State Design

The real-world proprioception is defined as $s_t^{p,real} \triangleq [q_{t-25:t}, \dot{q}_{t-25:t}, w_t^{root}, g_t, a_{t-25:t-1}]$ which contains the joint position q_t , joint velocity \dot{q}_t , root angular velocity w_t^{root} , projected gravity g_t and the last action a_{t-1} . We stack these terms over the last 25 steps to represent proprioception.

C. Control Interface and Mask Strategy

The distribution $p(s_t^{g,real} | s_t^{p,real})$ highly depends on how you collect and organize the pretraining dataset where goal states $s_t^{g,real}$ are introduced for each state-action pair $(s_t^{p,real}, a_t)$. One behavior may be specified by diverse control modes, resulting distinct goal states for current proprioception. For example, as is presented in figure 2.c, textual instruction, velocity command, whole-body joint positions as well as their arbitrary combinations constitute distinct control modes for specifying the behavior of walking forward. By activating diverse control modes, we actually draw goal state samples from the distribution $p(s_t^{g,real} | s_t^{p,real})$, which allows us to estimate the expectation over goal state distribution.

To simplify matters, we focus on low-level control modes that directly specifies the target state for root, kinematic positions and joint angles and design a control interface compatible with all these control modes, which contains:

- Root Control: target root translation, orientation (specified by RPY), linear velocity and angular velocity;
- Kinematic Position Control: target rigid-body positions of links rotated to the local frame of reference pose;
- Joint Angle Control: target joint angles for each motor;

By applying bit-wise binary mask to the control interface, we may activate distinct control modes for low-level control, allowing flexible and versatile control across diverse tasks.

In contrast to prior works [9] which adopt a two-stage mask strategy, we directly sample each element of the mask from a Bernoulli distribution $\mathcal{B}(0.5)$, facilitating application of arbitrary control modes. To ensure stable pretraining, we introduce a mask curriculum as a cold-start approach. The sampling probability for each Bernoulli trial gradually decays from an initial value of 1.0 towards 0.5 when the average episode length exceeds a predefined threshold. We adopt a relatively large decay factor in practice, resulting the cold-start phase to span only several hundred episodes.

D. Modeling BFM with Conditional Variational Autoencoder

We adopt a Conditional Variational Autoencoder (CVAE) to model the log-probability $\log P(a_t|s_t^{p,real}, s_t^{g,real})$. The Evidence Lower Bound (ELBO) of CVAE is expressed as:

$$\begin{aligned} & E_{q(z|s_t^{p,sim}, s_t^{g,sim})} [\log P(a_t|s_t^{p,real}, s_t^{g,real}, z)] \\ & - D_{KL}[q(z|s_t^{p,sim}, s_t^{g,sim})||P(z|s_t^{p,real}, s_t^{g,real})] \end{aligned} \quad (5)$$

We model the prior ρ , encoder ϵ and decoder D as Gaussian distributions and for the decoder, we assume it has a fixed variance. To encourage the latent space to encode more behavioral knowledge, we remove $s_t^{g,real}$ from the input of decoder. Following previous works [8, 22], we design the encoder to be a residual to the prior and include current mask m_t into the encoder input, which can be expressed as:

$$P(z|s_t^{p,real}, s_t^{g,real}) = \mathcal{N}(\mu^\rho(s_t^{p,real}, s_t^{g,real}), \sigma^\rho(s_t^{p,real}, s_t^{g,real})) \quad (6)$$

$$q(z|s_t^{p,sim}, s_t^{g,sim}) = \mathcal{N}(\mu^\epsilon(s_t^{p,sim}, s_t^{g,sim}, m_t) + \mu^\rho(s_t^{p,real}, s_t^{g,real}) \sigma^\epsilon(s_t^{p,sim}, s_t^{g,sim})) \quad (7)$$

$$P(a_t|s_t^{p,real}, s_t^{g,real}, z) = \mathcal{N}(\mu^D(s_t^{p,real}, z), \sigma_{fixed}) \quad (8)$$

E. Online Distillation

As we have prepared our behavioral dataset as a proxy agent, we employ the DAgger framework [23] to optimize the objective of BFM's pretraining. Specifically, for each episode, we roll out the current BFM $\pi_\theta(a_t|s_t^{p,real}, s_t^{g,real})$ in simulation to obtain trajectories of $(s_t^{p,real}, s_t^{g,real})$. At each timestep, we also compute the corresponding privileged states $(s_t^{p,sim}, s_t^{g,sim})$ and query the proxy agent for the reference action \hat{a}_t . Parameters of BFM is then updated by:

$$\begin{aligned} L_{DAgger} &= \|\hat{a}_t - a_t\|_2^2 \\ L_{KL} &= D_{KL}(q_\epsilon(z_t|s_t^{p,sim}, s_t^{g,sim})||P_\theta(z|s_t^{p,real}, s_t^{g,real})) \\ L &= L_{DAgger} + \lambda_{KL} L_{KL} \end{aligned} \quad (9)$$

where \hat{a}_t is the reference action from proxy agent, a_t is the action taken by current BFM, D_{KL} is the KL-Divergence operator and λ_{KL} maintains balance between the reconstruction quality and the latent space structural regularization. Domain randomization, termination conditions and hard negative mining strategy remain the same as proxy agent training.

V. BFM APPLICATION AND EXPERIMENTAL RESULTS

A. Experiment Setup

The training of our proxy agent and BFM is conducted in IsaacGym [24], with 8192 parallel environments. To ensure both the efficiency and persuasiveness of our evaluation, we report metrics calculated based on IsaacGym and demonstrate both the sim-to-sim results in Mujoco [25] and sim-to-real results in real world. We adopt the Unitree G1 humanoid robot [26] as an agile and powerful platform for real-world deployment, which stands 1.3 meters tall and has 29 degrees of freedom. To simplify the difficulty of control, we freeze the wrists of both hands, resulting in 23 degrees of freedom.

B. Steering BFM with the Control Interface

As our BFM enables humanoid control via diverse control modes, we first demonstrate its application of direct steering for multiple WBC tasks. We select three prevailing WBC tasks: whole-body motion tracking, VR teleoperation and locomotion to demonstrate the effectiveness of our BFM. For each task, we activate the corresponding control mode by manually crafting and applying mask to the control interface.

Baselines. To prove that our BFM has encoded extensive behavioral knowledge that can be directly steered by diverse WBC tasks, we select HOVER[9] as a general baseline for all the three tasks. For each task, we also select a specialist to show that our BFM is *as good as, if not better than*, the specialists for they often indicate overfitting to a specific control mode. We also train a BFM with the same architecture and hyper-parameters from scratch with reinforcement learning to ablate our options on the learning paradigm and the results of proxy agent are also included in the table for motion tracking and teleoperation. We select specialists with the same online distillation process and follows their implementation to align the training details which might vary from embodiment to dataset. For whole-body motion tracking, we follow the implementation of GMT [7] and for VR teleoperation, we refer to the implementation of OmniH2O [3]. We use our own implementation of specialists for the Locomotion task.

Metrics. For whole-body motion tracking and VR teleoperation, their goal is to track the control signals while demonstrating whole-body coordination. Therefore we adopt the same metric set for these two tasks comprised of the mean per-keypoint error (MPKPE) $E_{mpkpe}(mm)$, mean per-joint error (MPJPE) $E_{mpjpe}(rad)$, root linear velocity tracking error $E_{lin}(m/s)$ and angular velocity tracking error $E_{ang}(rad/s)$. For locomotion, its goal reduces to following a velocity command specified by root linear velocity on xy-plane and angular velocity along the z-axis. As a consequence, we adopt a metric set which contains the root linear velocity error on xy-plane $E_{lin,xy}$ and the root angular velocity error along z-axis $E_{ang,z}$. All the metrics are evaluated on three datasets, the training set of AMASS, the test set of AMASS and the 100STYLE dataset [27].

Experimental Results. As is demonstrated in Table III and IV, our BFM consistently outperforms HOVER on almost all metrics across all the tasks and datasets. Also, our BFM

TABLE III: Simulation evaluation of our BFM and baselines on **VR teleoperation** and **motion tracking** task. The most significant results are highlighted in bold and wrapped by dark background color and the second significant results are wrapped by light background color. For behavior modulation on motion tracking task, the results with the highest increments relative to our BFM are highlighted in bold and wrapped by dark background color. The results with increments relative to our BFM but not the most are wrapped by light background color.

Method	AMASS Train				AMASS Test				100Style			
	$E_{\text{mpjpe}} \downarrow$	$E_{\text{mpkpe}} \downarrow$	$E_{\text{lin}} \downarrow$	$E_{\text{ang}} \downarrow$	$E_{\text{mpjpe}} \downarrow$	$E_{\text{mpkpe}} \downarrow$	$E_{\text{lin}} \downarrow$	$E_{\text{ang}} \downarrow$	$E_{\text{mpjpe}} \downarrow$	$E_{\text{mpkpe}} \downarrow$	$E_{\text{lin}} \downarrow$	$E_{\text{ang}} \downarrow$
Proxy Agent	0.1864	49.3057	0.1469	0.9978	0.2137	56.1755	0.2631	1.3976	0.2460	64.1346	0.2036	1.2336
VR Teleoperation												
Specialist	0.2113	65.4214	0.2375	1.0925	0.2555	80.5919	0.4779	1.5036	0.3062	89.9115	0.3189	1.1525
HOVER	0.2676	91.2667	0.5047	1.6988	0.3055	102.8428	0.6468	1.8716	0.3455	119.8896	0.5351	1.6553
BFM (RL from Scratch)	1.0516	399.6902	0.4976	2.0627	1.1672	403.8327	0.6528	2.3211	1.1300	429.2893	0.4418	1.6848
BFM (Ours)	0.2447	72.3615	0.4006	1.2177	0.2235	63.1388	0.3066	1.4632	0.3169	87.0725	0.3238	1.1361
Motion Tracking												
Specialist	0.1895	53.9515	0.1586	1.0268	0.2247	73.6332	0.3034	1.4685	0.2491	67.7765	0.2128	1.2411
HOVER	0.2010	65.9742	0.2189	1.1599	0.2416	87.0678	0.3749	1.6554	0.2562	73.9817	0.2608	1.3369
BFM (RL from Scratch)	1.0503	400.1505	0.4973	2.0590	1.1689	404.7451	0.6533	2.3532	1.1215	429.5739	0.4422	1.6933
BFM (Ours)	0.1920	51.8372	0.1542	1.0142	0.2226	61.1236	0.3051	1.4358	0.2637	66.4027	0.2072	1.2790
Behavior Modulation on Motion Tracking												
$\lambda = 0.5$	0.1893	50.4801	0.1564	1.0419	0.2227	58.9844	0.2767	1.4099	0.2583	63.0582	0.2116	1.3394
$\lambda = 1.0$	0.1875	49.8647	0.1609	1.0681	0.2223	58.7251	0.2870	1.4899	0.2562	62.5168	0.2224	1.3919
$\lambda = 1.5$	0.1869	50.1451	0.1675	1.0866	0.2224	60.4565	0.2990	1.4964	0.2567	64.0520	0.2370	1.4618
$\lambda = 2.0$	0.2625	76.2392	0.2615	1.5176	0.2254	67.6583	0.3158	1.5438	0.2625	76.2392	0.2615	1.5176

TABLE IV: Simulation Evaluation of BFM and baselines on **locomotion** task across three datasets. The most significant results are highlighted in bold and wrapped by dark background color and the second significant results are wrapped by light background color.

Experiment	AMASS Train		AMASS Test		100Style	
	$E_{\text{lin,xy}} \downarrow$	$E_{\text{ang,z}} \downarrow$	$E_{\text{lin,xy}} \downarrow$	$E_{\text{ang,z}} \downarrow$	$E_{\text{lin,xy}} \downarrow$	$E_{\text{ang,z}} \downarrow$
Specialist	0.1201	0.4801	0.2168	0.6751	0.1496	0.5108
HOVER	0.1494	0.5518	0.2663	0.7624	0.1696	0.5707
BFM (RL from Scratch)	0.4314	1.2925	0.5513	1.4982	0.4015	1.0606
BFM (Ours)	0.1292	0.4974	0.2116	0.6744	0.1603	0.4973

is as good as, if no better than the specialists. We attribute the conditions where specialists may outperform our BFM to two reasons: 1) the specialists focus on a specific control mode, naturally allowing better learning of an unchanged setting. 2) the specialists may overfit to the training set under specific control mode. Besides, we observe that our BFM consistently outperforms the RL policy trained from scratch, which confirms that our training paradigm is effective for BFM pretraining. The overall results highlight our BFM’s versatility and generalization ability across multiple tasks.

C. Behavior Composition and Modulation with BFM

One key advantage of using a CVAE to model the BFM is that it provides a structured latent space that encodes a broad spectrum of behavioral knowledge. To fully unleash the potential of our BFM, we first perform latent analysis to clarify how the latent space has been structured. Then based on the analysis results, we further perform experiments to demonstrate some unique and special properties of our BFM.

Latent Structure. We first choose five motions including standing still, walking forward, walking backward, left

sidestep and right sidestep. Then we adopt the control mode of motion tracking to collect latent sequences and apply the t-SNE algorithm [28] to project the high-dimensional latent variables into a 2D plane for visualization. As shown in figure 3.b, we observe that 1) the projected latent variables demonstrate clear directionality and symmetry. 2) While humanoids are all initialized as the same standing pose, the latent variables are pre-clustered instead of transiting from center to diverse directions, indicating our model may have learned strong prior over latent space. Overall, this analysis confirms that the CVAE learns a meaningful and structured latent manifold, which can be leveraged for diverse purposes.

Behavior Composition. We explore the possibility of interpolation in the latent space for producing novel behaviors. We select the Roundhouse Kick as a difficult motion to perform and activates the control mode of root and keypoint separately. We observe that root-only control leads to a turning movement without raising leg while keypoint-only control results in raising leg without turning around. However, when we linearly interpolate the latent variables from these two control modes with a coefficient of 0.5, the humanoid could complete the Roundhouse Kick motion, as is demonstrated in figure 3.a. By gradually increasing the coefficient from 0 to 1, the humanoid exhibits a clear transition among root-only control, full completion and keypoint-only control. The overall results highlight the structure our BFM has acquired which allows flexible compositions of diverse behaviors.

Behavior Modulation. We further explore the possibility of extrapolation in the latent space for better alignment with desired mode. We select the Butterfly Kick as a challenging motion the model fails to directly perform under the motion tracking mode, where it will lose its balance when landing on the ground. We propose to obtain latent variables in a similar

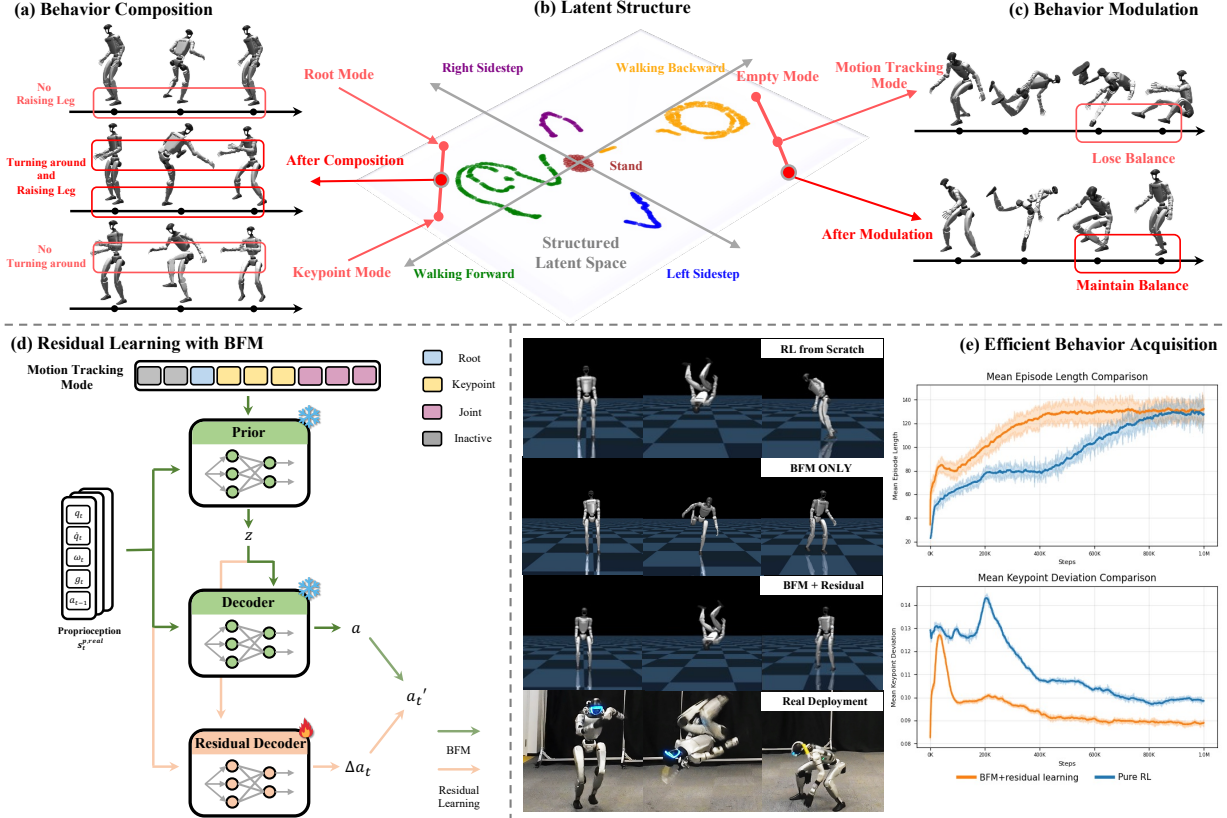


Fig. 3: (a) BFM allows behavior composition for novel behaviors through linear interpolation of latent variables from two distinct control modes. (b) T-SNE results (brown for standing, green for walking forward, yellow for walking backward, blue for left sidestep and purple for right sidestep) demonstrates our BFM provides a structured latent space with clear directionality and symmetry. (c) BFM allows behavior modulation to better align with desired control modes through linear extrapolation in the latent space. (d) We adopt residual learning on our pretrained BFM for efficient acquisition of novel behaviors. (e) We select Side Salto as a challenging case and compare our method with training RL policy from scratch.

way to Classifier-free Guidance [29] in Diffusion models:

$$z = (1 + \lambda)\mu^\rho(s_t^{p,real}, s_t^{g,real}) - \lambda\mu^\rho(s_t^{p,real}, \emptyset), \lambda > 0 \quad (10)$$

We find that by setting λ as 0.5, the humanoid can now maintain its balance when landing, as is demonstrated in figure 3.c. To further clarify its effect, we apply this finding to the motion tracking task. As is presented in table III, when applying a medium coefficient, the tracking results all achieve improvements to some extent. While a relatively large coefficient may lead to degradation of performance, indicating an excessive modulation towards the control mode.

D. Efficient Behavior Acquisition with BFM

By pretraining over large-scale behavioral dataset, our BFM is equipped with sufficient behavioral knowledge for efficient acquisition of novel behaviors. By focusing on novel behaviors specified by reference motions, we still adopt motion imitation as an effective paradigm for behavior learning. Specifically, we freeze all the parameters of BFM and activate the control mode of motion tracking. Upon our pretrained model, we learn a residual decoder $\pi(\Delta a_t | s_t^{p,real}, z)$ and the final action becomes $a'_t = a_t + \Delta a_t$, as is presented in figure 3.d. The training of residual model follows the same configuration as the proxy agent, except we activate termination curriculum [6] and adjust the threshold

based on the sequence length of each motion. To demonstrate the effectiveness of residual learning, we select side salto as a challenging motion that the BFM can not directly handle and present the visualization results and curves for mean keypoint deviations and mean episode lengths. As is shown in figure 3.e, by comparing our methods of residual learning on BFM with methods of learning RL policy from scratch, the existence of BFM avoids inefficient exploration at early stage of training and achieves more accurate tracking results based on the behavioral knowledge our BFM has learned.

VI. CONCLUSION

In this work, we introduce Behavior Foundation Model for humanoid robots, a generative model for behaviors pre-trained on large-scale behavioral dataset to encode extensive, reusable behavioral knowledge. Based on mathematical analysis under RL formulation, we implement our BFM through the training of a proxy agent and online masked distillation by a CVAE. Comprehensive evaluations consolidate that our BFM achieves strong capabilities of cross-task generalization, behavior composition, behavior modulation and efficient acquisition of novel behaviors. Future work may further extend the current simplified control interface to support a broader range of control modes.

REFERENCES

- [1] Z. Jiang, Y. Xie, J. Li, Y. Yuan, Y. Zhu, and Y. Zhu, “Harmon: Whole-body motion generation of humanoid robots from language descriptions,” *arXiv preprint arXiv:2410.12773*, 2024.
- [2] Y. Shao et al., “Langwbc: Language-directed humanoid whole-body control via end-to-end learning,” *arXiv preprint arXiv:2504.21738*, 2025.
- [3] T. He et al., “Omnih2o: Universal and dexterous human-to-humanoid whole-body teleoperation and learning,” *arXiv preprint arXiv:2406.08858*, 2024.
- [4] Q. Ben, F. Jia, J. Zeng, J. Dong, D. Lin, and J. Pang, “Homie: Humanoid loco-manipulation with isomorphic exoskeleton cockpit,” *arXiv preprint arXiv:2502.13013*, 2025.
- [5] C. Lu et al., “Mobile-television: Predictive motion priors for humanoid whole-body control,” in *2025 IEEE International Conference on Robotics and Automation (ICRA)*, IEEE, 2025, pp. 5364–5371.
- [6] T. He et al., “Asap: Aligning simulation and real-world physics for learning agile humanoid whole-body skills,” *arXiv preprint arXiv:2502.01143*, 2025.
- [7] Z. Chen, M. Ji, X. Cheng, X. Peng, X. B. Peng, and X. Wang, “Gmt: General motion tracking for humanoid whole-body control,” *arXiv preprint arXiv:2506.14770*, 2025.
- [8] C. Tessler, Y. Guo, O. Nabati, G. Chechik, and X. B. Peng, “Maskedmimic: Unified physics-based character control through masked motion inpainting,” *ACM Transactions on Graphics (TOG)*, vol. 43, no. 6, pp. 1–21, 2024.
- [9] T. He et al., “Hover: Versatile neural whole-body controller for humanoid robots,” in *2025 IEEE International Conference on Robotics and Automation (ICRA)*, IEEE, 2025, pp. 9989–9996.
- [10] A. Radford, J. Wu, R. Child, D. Luan, D. Amodei, I. Sutskever, et al., “Language models are unsupervised multitask learners,” *OpenAI blog*, vol. 1, no. 8, p. 9, 2019.
- [11] I. Higgins et al., “Beta-vae: Learning basic visual concepts with a constrained variational framework,” in *International conference on learning representations*, 2017.
- [12] K. He, X. Zhang, S. Ren, and J. Sun, “Deep residual learning for image recognition,” in *Proceedings of the IEEE conference on computer vision and pattern recognition*, 2016, pp. 770–778.
- [13] Y. Xue, W. Dong, M. Liu[†], W. Zhang, and J. Pang, “A unified and general humanoid whole-body controller for versatile locomotion,” *arXiv preprint arXiv:2502.03206*, 2025.
- [14] Y. Ze et al., “Twist: Teleoperated whole-body imitation system,” *arXiv preprint arXiv:2505.02833*, 2025.
- [15] A. Tirinzoni et al., “Zero-shot whole-body humanoid control via behavioral foundation models,” *arXiv preprint arXiv:2504.11054*, 2025.
- [16] J. Schulman, F. Wolski, P. Dhariwal, A. Radford, and O. Klimov, “Proximal policy optimization algorithms,” *arXiv preprint arXiv:1707.06347*, 2017.
- [17] N. Mahmood, N. Ghorbani, N. F. Troje, G. Pons-Moll, and M. J. Black, “Amass: Archive of motion capture as surface shapes,” in *Proceedings of the IEEE/CVF international conference on computer vision*, 2019, pp. 5442–5451.
- [18] M. Loper, N. Mahmood, J. Romero, G. Pons-Moll, and M. J. Black, “Smpl: A skinned multi-person linear model,” in *Seminal Graphics Papers: Pushing the Boundaries, Volume 2*, 2023, pp. 851–866.
- [19] T. He et al., “Learning human-to-humanoid real-time whole-body teleoperation,” in *2024 IEEE/RSJ International Conference on Intelligent Robots and Systems (IROS)*, IEEE, 2024, pp. 8944–8951.
- [20] L. Campanaro, S. Gangapurwala, W. Merkt, and I. Havoutis, “Learning and deploying robust locomotion policies with minimal dynamics randomization,” in *6th Annual Learning for Dynamics & Control Conference*, PMLR, 2024, pp. 578–590.
- [21] X. B. Peng, P. Abbeel, S. Levine, and M. Van de Panne, “Deepmimic: Example-guided deep reinforcement learning of physics-based character skills,” *ACM Transactions On Graphics (TOG)*, vol. 37, no. 4, pp. 1–14, 2018.
- [22] H. Yao, Z. Song, B. Chen, and L. Liu, “Controlvae: Model-based learning of generative controllers for physics-based characters,” *ACM Transactions on Graphics (TOG)*, vol. 41, no. 6, pp. 1–16, 2022.
- [23] S. Ross, G. Gordon, and D. Bagnell, “A reduction of imitation learning and structured prediction to no-regret online learning,” in *Proceedings of the fourteenth international conference on artificial intelligence and statistics*, JMLR Workshop and Conference Proceedings, 2011, pp. 627–635.
- [24] V. Makoviychuk et al., “Isaac gym: High performance gpu-based physics simulation for robot learning,” *arXiv preprint arXiv:2108.10470*, 2021.
- [25] E. Todorov, T. Erez, and Y. Tassa, “Mujoco: A physics engine for model-based control,” in *2012 IEEE/RSJ international conference on intelligent robots and systems*, IEEE, 2012, pp. 5026–5033.
- [26] Unitree, *Unitree g1 humanoid agent ai avatar*, 2024.
- [27] I. Mason, S. Starke, and T. Komura, “Real-time style modelling of human locomotion via feature-wise transformations and local motion phases,” *Proceedings of the ACM on Computer Graphics and Interactive Techniques*, vol. 5, no. 1, May 2022.
- [28] L. v. d. Maaten and G. Hinton, “Visualizing data using t-sne,” *Journal of machine learning research*, vol. 9, no. Nov, pp. 2579–2605, 2008.
- [29] J. Ho and T. Salimans, “Classifier-free diffusion guidance,” *arXiv preprint arXiv:2207.12598*, 2022.